Advanced Ceramics Progress: Vol. 8, No. 3, (Summer 2022) 1-7

Materials and Energy Research Center
MERC

Contents lists available at ACERP

Advanced Ceramics Progress

Journal Homepage: www.acerp.ir

Original Research Article

Studying the Effect of Calcination on the Optical and Magnetic Properties of $NiFe_2O_4$@ZnO:Ti Nanoparticles

Zahra Abdi [a], Adrine Malek Khachatourian [b,*], Ali Nemati [c]

[a] *MSc, Department of Materials Science and Engineering, Sharif University of Technology, Tehran, Tehran, Iran*
[b] *Assistant Professor, Department of Materials Science and Engineering, Sharif University of Technology, Tehran, Tehran, Iran*
[c] *Professor, Department of Materials Science and Engineering, Sharif University of Technology, Tehran, Tehran, Iran*

* Corresponding Author Email: khachatourian@sharif.edu (A. Malek Khachatourian)

URL: https://www.acerp.ir/article_159438.html

ARTICLE INFO

Article History:

Received 22 september 2022
Received in revised form 19 October 2022
Accepted 24 October 2022

Keywords:

Magnetic Nanoparticles
Heterogeneous Nucleation
Hydrothermal Method
Band Gap Engineering
Saturation Magnetization

ABSTRACT

In this study, novel magnetically separable $NiFe_2O_4$@ZnO:Ti nanospheres were synthesized using the heterogeneous nucleation of ZnO:Ti (Ti-doped ZnO) nanoparticles on $NiFe_2O_4$ polycrystalline nanospheres through the hydrothermal method. Structural and microstructural properties of the synthesized polycrystalline nanospheres were investigated through Fourier-Transform Infrared Spectra (FTIR), X-Ray Diffraction (XRD), Transmission Electron Microscopy (TEM), and Field Emission Scanning Electron Microscopy (FESEM) using an Energy-Dispersive X-ray (EDX) spectrometer. The effect of calcination on the magnetic and optical properties was also studied. The optical features of the synthesized nanoparticles were recorded using UV-Vis spectroscopy, indicating the absorption peak in the visible region. The band gap energy of pure ZnO, ZnO:Ti, and $NiFe_2O_4$@ZnO:Ti before and after calcination was calculated as 3.21 eV, 2.92 eV, 2.44 eV, and 2.04 eV, respectively. Further, Vibrating Sample Magnetometer (VSM) was employed to examine the magnetic features, and the saturation magnetization (Ms) values of $NiFe_2O_4$ and $NiFe_2O_4$@ZnO:Ti non-calcined and calcined were obtained as 63.6 emu/g, 21.3 emu/g, and 15.3 emu/g, respectively. The findings revealed that calcination of $NiFe_2O_4$@ZnO:Ti nanospheres improved the optical properties and reduced the band gap energy. However, $NiFe_2O_4$ combination with nonmagnetic matrix and calcination of $NiFe_2O_4$@ZnO:Ti nanoparticles decreased the Ms value and response to the external magnetic field.

https://doi.org/10.30501/acp.2022.363261.1101

1. INTRODUCTION

Considerable attention has been recently drawn to semiconductor nanomaterials and spinel ferrite nanocrystals due to their wide applications such as photocatalytic degradation of dyes, photoelectric devices, adsorption-membrane filtration, and sensors due to their excellent optical and magnetic features [1,2]. A remarkable semiconductor, Zinc oxide (ZnO), has been frequently used in recent years due to its high potential of charge carriers between the conduction band and valence band under light energy. Nevertheless, the wide band gap energy (~ 3.37 eV) and excitation under UV radiation that forms only about 10 percent of solar light are significant drawbacks of ZnO nanoparticles [3,4]. Many strategies, namely doping different atoms and coupling with other compounds, were suggested to improve the optical properties of these nanoparticles. Doping

Please cite this article as: Abdi, Z., Malek Khachatourian, A., Nemati, A., "Studying the Effect of Calcination on the Optical and Magnetic Properties of $NiFe_2O_4$@ZnO:Ti Nanoparticles", ***Advanced Ceramics Progress***, Vol. 8, No. 3, (2022), 1-7. https://doi.org/10.30501/acp.2022.363261.1101

transition metals such as Fe, Ni, and Cu into the ZnO crystal structure reduces the band gap energy level and modifies the electronic structure. When the nanomaterials like CuO, CeO_2, and $ZnFe_2O_4$ couple with ZnO nanoparticles, a new band gap energy level is formed for easy separation of photoinduced electrons in the visible light region [5-9]. Spinel ferrite MFe_2O_4 (M = Mn, Fe, Co, Ni, …) nanomaterials with high chemical stability and large surface area are characterized by remarkable superparamagnetic properties [10-12]. In addition, coupling spinel ferrite nanomaterials with semiconductors help reduce the band gap energy and easy separation of catalysts under an external magnetic field. Garima Vaish et al. [13]. synthesized $MgFe_2O_4/TiO_2$ nanocomposites using the economic ultra-sonication method and identified appropriate magnetic and optical properties for magnetic, photocatalytic, and optoelectronic devices.

The present study aimed to synthesize novel magnetic $NiFe_2O_4$@ZnO:Ti nanoparticles using an in-situ hydrothermal method and evaluate the effects of calcination on nanocomposite optical and magnetic properties. Monodisperse spherical $NiFe_2O_4$ nanoparticles exhibit high water solubility and large saturation magnetization (Ms) due to Polyacrylamide (PAM) as a hydrophilic polymer in the hydrothermal process. Doping titanium atoms modify the band gap energy of ZnO nanoparticles. Further, coupling ZnO:Ti (Ti-doped ZnO) nanoparticles with $NiFe_2O_4$ nanospheres improves the optical properties and exhibits magnetic properties. Subsequently, magnetic and optical features of $NiFe_2O_4$@ZnO:Ti nanospheres were studied before and after calcination at 500 °C by UV-Vis spectroscopy and VSM analysis.

2. MATERIALS AND METHODS

2.1. Materials

Nickel (II) chloride ($NiCl_2.6H_2O$), PAM, Mn=150000) $(C_3H_5NO)_n$, iron (III) chloride ($FeCl_3.6H_2O$), sodium citrate ($Na_3C_6H_5O_7.2H_2O$), urea (CH_4N_2O), and ethanol (C_2H_6O) were purchased from Merck Company (Germany) to prepare $NiFe_2O_4$ nanoparticles. Potassium hydroxide (KOH), methanol (CH_3OH), zinc acetate dihydrate ($Zn(CH_3COO)_2.2H_2O$), and Titanium Isopropoxide (TTIP) ($C_{12}H_{28}O_4Ti$) were also bought from Merck Company to fabricate ZnO:Ti nanoparticles.

2.2. Synthesis of $NiFe_2O_4$

The super-paramagnetic $NiFe_2O_4$ nanoparticles were synthesized through a modified hydrothermal method [14]. $FeCl_3{\cdot}6H_2O$ (1 mmol) and $NiCl_2{\cdot}6H_2O$ (0.5 mmol) were added into 40 mL distilled water. Then, sodium citrate (3 mmol), urea (6 mmol), and PAM (0.3 g) were dissolved in the resultant solution, respectively. The green obtained solution was stirred continuously until PAM was entirely disintegrated. After a specific time, the resulting solution was poured into a Teflon-lined autoclave and maintained for 12 hours in an oven at 200 °C. Then, the brownish solution was centrifuged, washed several times with ethanol and distilled water, and left in an oven at 60 °C for three hours.

2.3. Synthesis of $NiFe_2O_4$@ZnO:Ti Nanoparticles

A hydrothermal technique was employed to fabricate $NiFe_2O_4$@ZnO:Ti nanospheres. In a typical preparation, zinc acetate dihydrate (1.25 mmol) was dispersed in 40 mL methanol, and potassium hydroxide (2 mmol) was added to this solution to adjust pH = 8. Then, 7.5 wt. % of TTIP was put into the solution and stirred vigorously. Next, 0.04 g of the as-prepared magnetic $NiFe_2O_4$ nanoparticles was sonicated and poured into the above solution. The mixture was refluxed for five hours at 70 °C. Once the reaction was completed, the obtained solution was hydrothermally processed in a Teflon-lined stainless-steel autoclave for 12 hours at 180 °C. The synthetic powders were gathered by centrifugation, washed several time with deionized water (DI), and maintained in an oven at 60 °C. Of note, ZnO and ZnO:Ti nanoparticles were also synthesized without a $NiFe_2O_4$ core with the same method as that used for the reference powders.

2.4. Characterization

The X-Ray Diffraction (XRD) patterns of the powder were obtained using a multipurpose X-ray diffractometer (PANalytical X'Pert Pro MPD) with Cu K_α radiation (λ = 1.5406 Å). In addition, Fourier-Transform Infrared spectroscopy (FTIR; Perkin Elmer-Spectrum 65) was employed to study the functional groups of the samples. The microstructure and chemical composition of the samples were investigated using (TEM; Philips EM208S-100 kV) and (FE-SEM; TESCAN company, MIRA3) with an Energy-Dispersive X-ray Spectrometer (EDS). The magnetic features were evaluated by a vibrating sample magnetometer (VSM; MDK company). In addition, a UV-Vis spectrophotometer (JENWAY 6705) was utilized to assess the optical properties.

3. RESULTS AND DISCUSSION

3.1. XRD Analysis

Fig. 1 depicts the XRD patterns of ZnO, ZnO:Ti, $NiFe_2O_4$, and $NiFe_2O_4$@ZnO:Ti nanoparticles to study the crystalline structure and phase identification. In the XRD pattern of pure ZnO (Fig. 1a), the diffraction peaks were observed at 2θ = 31.8°, 34.5°, 36.3°, 47.6°, 56.7°, 62.9°, 66.4°, 68.0°, and 69.2° attributed to (100), (002), (101), (102), (110), (103), (200), (112), and (201) crystal planes of typical hexagonal wurtzite phase (JCPDS file no. 36-1451) [15]. After doping Ti, the same peaks were detected in the XRD pattern of ZnO:Ti, and insignificant

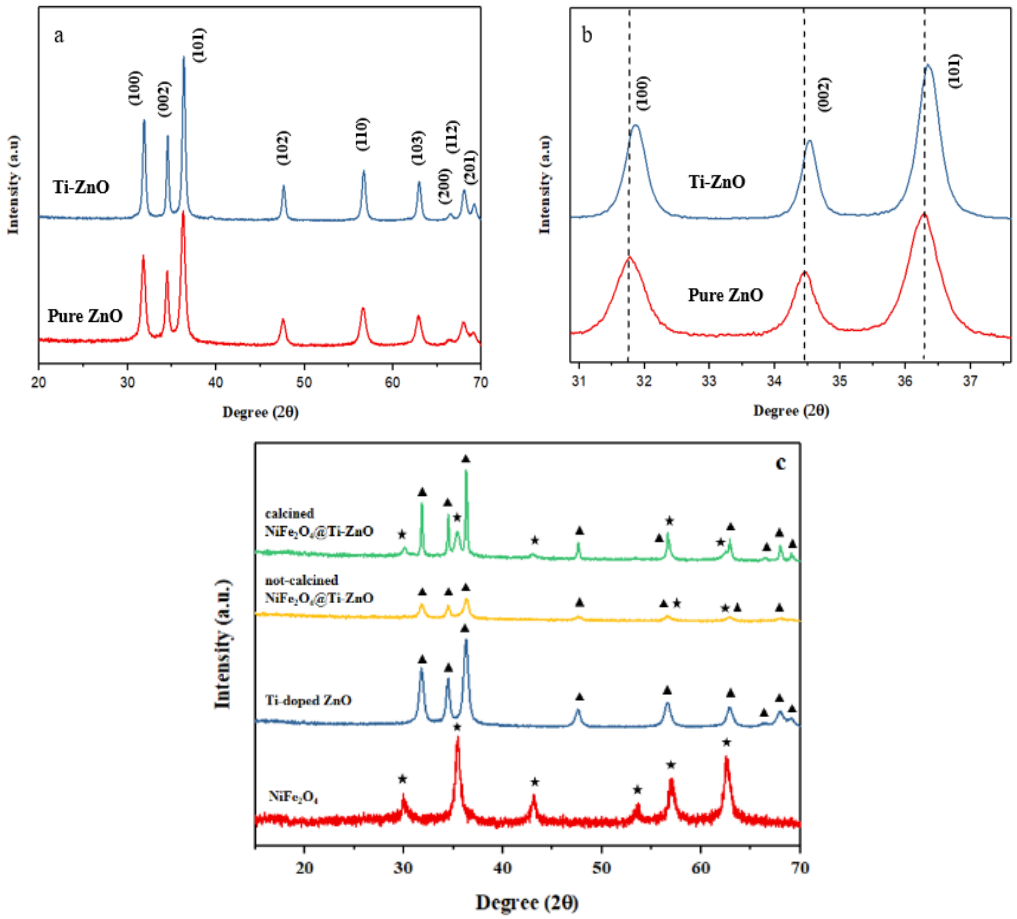

Figure 1. XRD patterns of (a-b) pure ZnO and ZnO:Ti, and (c) non-calcined and calcined $NiFe_2O_4$@ZnO:Ti

peak shifting occurred due to the diversity of the ionic radius between Ti^{4+} (0.068 nm) and Zn^{2+} (0.074 nm) (Fig. 1b). As demonstrated in Fig. 1c, the diffraction peaks of $NiFe_2O_4$ revealed 2θ = 29.9°, 35.4°, 43.2°, 53.5°, 56.8°, 62.7° refer to (220), (311), (400), (422), (511), and (440) crystal planes, thus proving the formation of pure spinel phase (JCPDS file no. 19–0629) [16]. Further, the mean grain sizes (D) of ZnO, ZnO:Ti, and $NiFe_2O_4$ nanoparticles were measured through the Scherrer equation [17]:

$$D = \frac{k\lambda}{\beta \cos\theta} \quad (1)$$

where k denotes the shape factor whose value was measured as approximately 0.9, λ the wavelength of X-ray, θ the Bragg's diffraction angle, and β the diffraction peak width at the half maximum (FWHM). Table. 1 lists the obtained grain sizes of the powders. The XRD pattern of $NiFe_2O_4$@ZnO:Ti nanoparticles (Fig. 1c) shows the same diffraction peaks of the $NiFe_2O_4$ and ZnO:Ti nanoparticles without any extra peaks, thus confirming the thorough formation of $NiFe_2O_4$@ZnO:Ti nanospheres. However, in the XRD pattern of the calcined $NiFe_2O_4$@ZnO:Ti, the diffraction peaks of $NiFe_2O_4$ and ZnO:Ti appeared distinctly with higher intensity than that of the peaks of non-calcined nanoparticles.

3.2. FTIR Analysis

The functional groups of $NiFe_2O_4$, ZnO:Ti, and $NiFe_2O_4$@ZnO:Ti nanoparticles were assessed using the FTIR spectroscopy (Fig. 2). For all the prepared samples spectra, the O–H stretching vibration band appeared at about 3400 cm^{-1}. In the FTIR spectrum of $NiFe_2O_4$, Fe–O stretching at 595 cm^{-1}, NH_2 deformation bands at 1656 cm^{-1}, and CH_2 deformation band at 1410 cm^{-1} were detected that were attributed to the presence of the PAM in the process of synthesis [18]. The characteristic peak at 526 cm^{-1} is relevant to the Zn–O stretching band, and the main characteristic peaks at 1348 cm^{-1}, 1419 cm^{-1}, and 1626 cm^{-1} related to the C=O mode of zinc acetate were observed in the FTIR spectrum of ZnO:Ti [19]. Eventually, all the characteristic peaks of $NiFe_2O_4$ and ZnO:Ti nanoparticles appeared in the non-calcined $NiFe_2O_4$@ZnO:Ti spectrum.

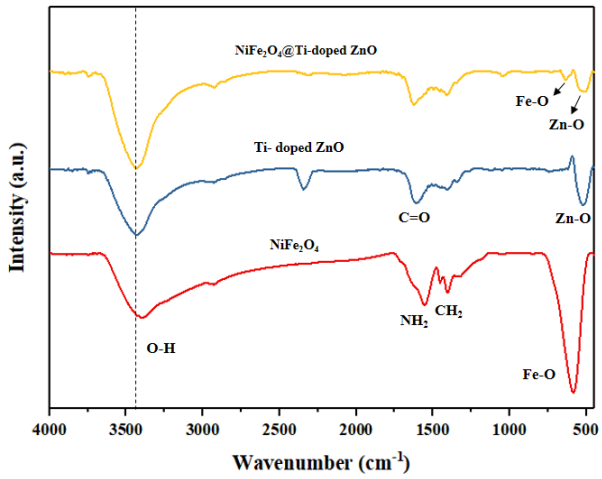

Figure 2. FTIR spectrum of $NiFe_2O_4$, ZnO:Ti, and non-calcined $NiFe_2O_4$@ZnO:Ti

3.3. Microstructure Analysis

The microstructure, chemical composition, and surface morphology of the as-prepared samples were analyzed using FE-SEM and EDS analyses. As shown in Fig. 3a, the ZnO:Ti nanoparticles are characterized by similar spherical morphology with the mean particle size of 27 nm. The FESEM images of $NiFe_2O_4$ (Fig. 3b) indicated well-distribution spherical nanoparticles with the mean particle size of 200 nm. In addition, the presence of PAM and citrate in the hydrothermal process led to the formation of monodisperse nanospheres and prevented random aggregation of $NiFe_2O_4$ nanoparticles. Fig. 3c vividly illustrates the deposition of ZnO:Ti nanoparticles into the $NiFe_2O_4$ nanospheres and coarsening of its surface. Moreover, the particle size of non-calcined $NiFe_2O_4$@ZnO:Ti increased up to around 230 nm. As demonstrated in Fig. 4, the FESEM e-maps of the Energy-Dispersive X-ray spectroscopy (EDS) of non-calcined $NiFe_2O_4$@ZnO:Ti proved the presence of Ni, Fe, O, Zn, and Ti with homogeneous distribution.

The EDS spectra of the sample also confirmed the presence of K atoms that attribute to KOH to adjust the pH. The clear morphological images of non-calcined $NiFe_2O_4$@ZnO:Ti nanoparticles were included in the TEM analysis (Fig. 5). The TEM images of powders confirmed the growth of a thin layer of ZnO:Ti nanoparticles on the polycrystalline spherical $NiFe_2O_4$ nanoparticles.

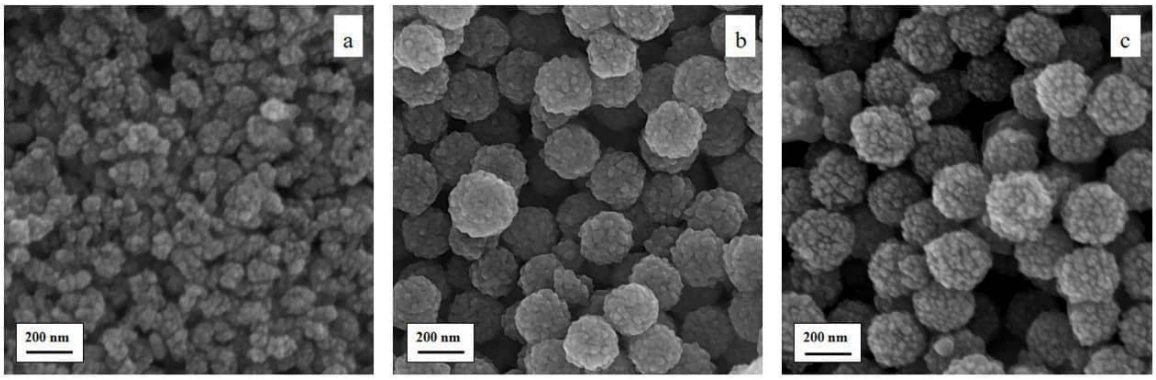

Figure 3. FE-SEM images of (a) ZnO:Ti (b) $NiFe_2O_4$, and (c) non-calcined ZnO:Ti@$NiFe_2O_4$

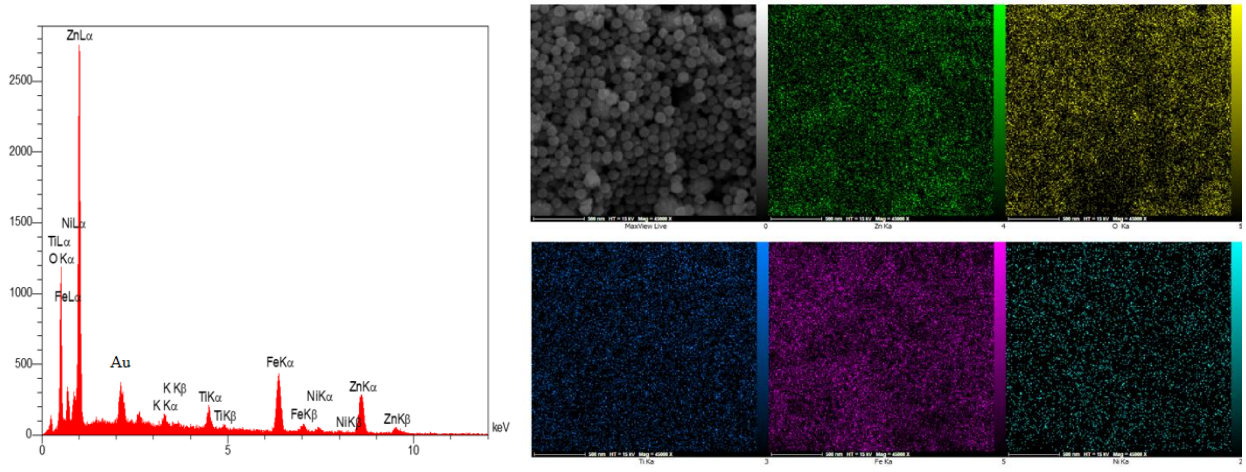

Figure 4. EDS spectrum and elemental mapping of non-calcined ZnO:Ti@$NiFe_2O_4$

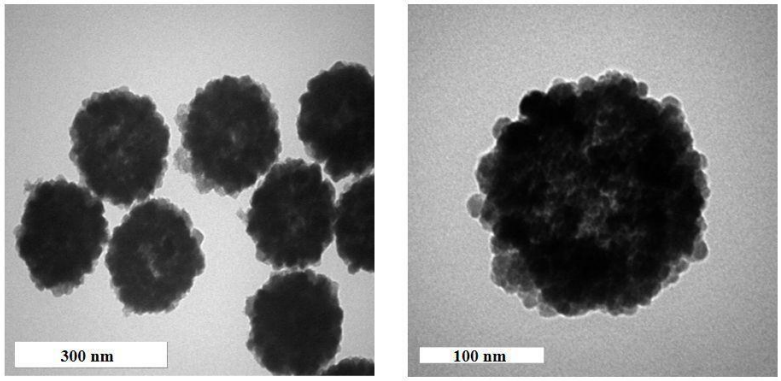

Figure 5. TEM images of non-calcined ZnO:Ti@$NiFe_2O_4$ nanoparticles

3.4. UV-Vis Analysis

The optical features of ZnO, ZnO:Ti, and non-calcined and calcined $NiFe_2O_4$@ZnO:Ti nanoparticles were investigated using UV-Vis spectrometry. As shown in Fig. 6a, pure ZnO can be simulated in the ultraviolet region at 385 nm. However, the absorption peak of ZnO:Ti nanoparticles tuned to the visible region at 456 nm. For $NiFe_2O_4$@ZnO:Ti nanoparticles before and after calcination, the absorption peaks have redshift to the visible region at about 500 nm. The optical bandgap energy (E_g) of the samples was obtained using Tauc relation [20]:

$$(\alpha h\upsilon)^2 = A(h\upsilon - E_g) \quad (2)$$

where $h\upsilon$ stands for the photon energy, α the absorption coefficient, and A a constant. Fig. 6b illustrates the plot of $(\alpha h\nu)^2$ as a function of $h\upsilon$. The band gap value of ZnO decreased after doping Ti, coupling with $NiFe_2O_4$, and calcination at 500 °C (as summarized in Table. 1).

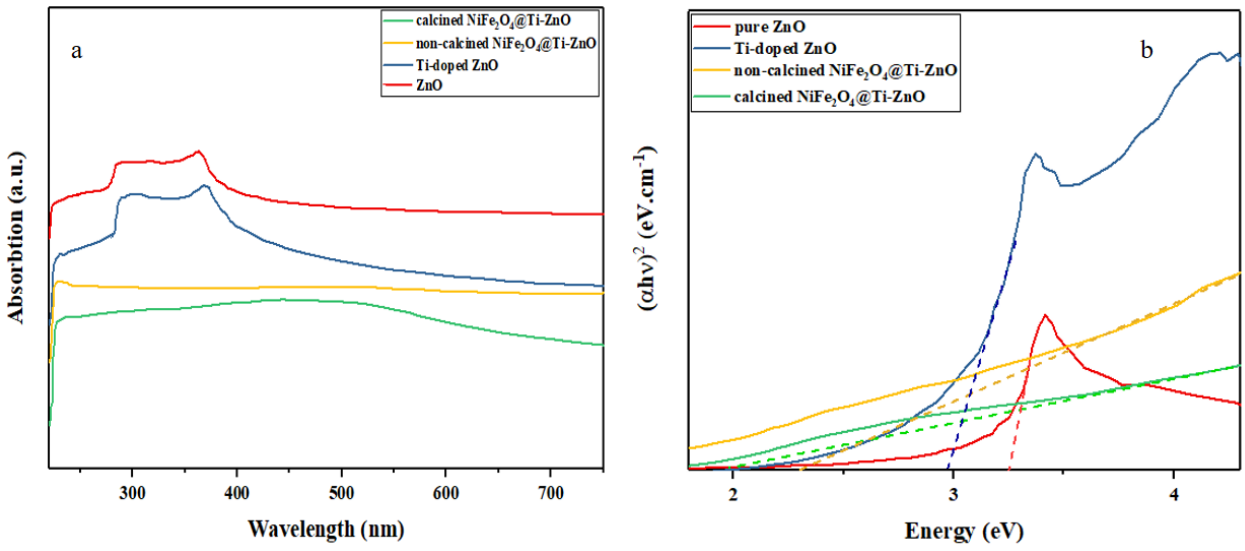

Figure 6. (a) UV-Vis spectrum and (b) Kubelka-Munk plots of samples

TABLE 1. Crystallite size (D), Particle size, Bandgap energies, Ms

Samples	Crystallite Size (nm)	Particle Size (nm)	Band Gap (eV)	Ms (emu/g)
	XRD	SEM	UV-Visible Spectra	VSM
$NiFe_2O_4$	11	200	-	63.6
Pure ZnO	27	38	3.21	-
Ti-Doped ZnO	14	27	2.92	-
Non-Calcined $NiFe_2O_4$@Ti-doped ZnO	-	230	2.44	21.3
Calcined $NiFe_2O_4$@Ti-doped ZnO	-	-	2.04	15.3

According to the results, the bandgap of $NiFe_2O_4$@ZnO:Ti nanoparticles after calcination reached 2.04 eV. Of note, calcination significantly decreased the band gap energy because of the improvement in the substantial oxygen vacancy defects.

3.5. VSM Analysis

The magnetic features of $NiFe_2O_4$, non-calcined $NiFe_2O_4$@ZnO:Ti, and calcined $NiFe_2O_4$@ZnO:Ti were recorded using VSM analysis. Fig. 7 shows the magnetic hysteresis curves of all samples with no coercivity or definite remnant magnetization that exhibits superparamagnetic behavior at room temperature.

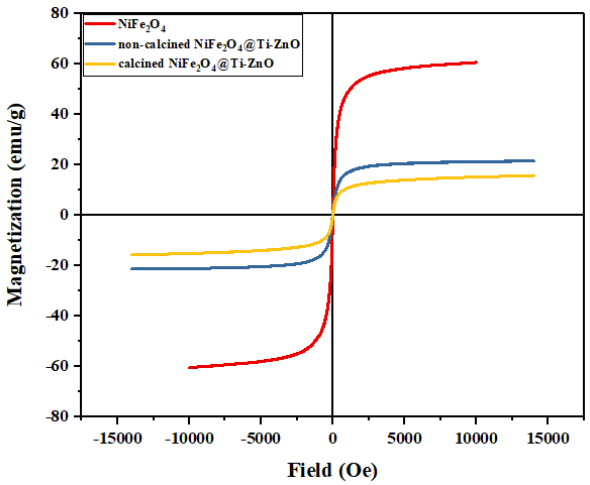

Figure 7. Magnetic hysteresis loops of the samples

Pure $NiFe_2O_4$ nanoparticles are characterized by a high Ms value of 63.6 emu/g (applied field sweeping from −10 K to 10 K Oe) due to their small crystallite size. Furthermore, $NiFe_2O_4$ composition with ZnO:Ti as a non-magnetic material decreased Ms value to 21.3 emu/g (applied field sweeping from −15 K to 15 K Oe). As a result of calcination on the magnetic features of $NiFe_2O_4$@ZnO:Ti nanoparticles, the Ms value was reduced by 15.1 emu/g (applied field sweeping from −15 K to 15 K Oe) due to the increasing crystallite size, non-uniform particle distribution, and decreasing the surface to volume ratio.

4. CONCLUSION

The magnetically separable $NiFe_2O_4$@ZnO:Ti nanoparticles were successfully synthesized using one-step hydrothermal methods. The optical and magnetic features of the prepared samples were examined through the UV-Vis analysis, Kubelka-Munk plots, and VSM analysis. The $NiFe_2O_4$@ZnO:Ti nanoparticles can be excited in the visible region. Additionally, the band gap value of pure ZnO decreased from 3.21 eV to 2.44 eV for $NiFe_2O_4$@ZnO:Ti nanoparticles. Improvement in the optical properties in the visible reign and decrease in the band gap energy value by 2.04 eV were noticed followed by calcination of $NiFe_2O_4$@ZnO:Ti. In addition, the Ms value of superparamagnetic $NiFe_2O_4$ reduced from 63.6 emu/g to 15.1 emu/g after coupling with ZnO:Ti and calcination at 500 °C. However, the as-prepared nanoparticles exhibited an appropriate response to the external magnetic field.

It should be noted that $NiFe_2O_4$@ZnO:Ti nanoparticles exhibited proper photocatalytic performance, hence widely used in environmental applications and wastewater treatment. Moreover, the composition of these nanoparticles with graphene and different polymers could improve the photocatalytic activity under visible light.

ACKNOWLEDGEMENTS

The authors would like to acknowledge Sharif University of Technology for supporting this research.

NOMENCLATURE

$\propto$	Absorption coefficient
A	A constant
β	Diffraction peak width at half maximum (FWHM)
D	Average grain size
Eg	Optical bandgap energy
Eq.	Equation
$h\upsilon$	Photon energy
k	Shape factor
Ms	Saturation magnetization
θ	Natural logarithm of MSW generation
λ	Natural logarithm of population

REFERENCES

1. Reddy, D. H. K., Yun, Y. S., “Spinel ferrite magnetic adsorbents: alternative future materials for water purification?”, ***Coordination Chemistry Reviews***, Vol. 315, (2016), 90-111. https://doi.org/10.1016/j.ccr.2016.01.012
2. Terna, A. D., Elemike, E. E., Mbonu, J. I., Osafile, O. E., Ezeani, R. O., “The future of semiconductors nanoparticles: Synthesis, properties and applications”, ***Materials Science and Engineering: B***, Vol. 272, (2021), 115363. https://doi.org/10.1016/j.mseb.2021.115363
3. Caglar, M., Ilican, S., Caglar, Y., Yakuphanoglu, F., “Electrical conductivity and optical properties of ZnO nanostructured thin film.”, ***Applied Surface Science***, Vol. 255, No. 8, (2009), 4491-4496. https://doi.org/10.1016/j.apsusc.2008.11.055
4. Noman, M. T., Amor, N., Petru, M., “Synthesis and applications of ZnO nanostructures (ZONSs): a review”, ***Critical Reviews in Solid State and Materials Sciences***, Vol. 47, No. 2, (2022), 99-141. https://doi.org/10.1080/10408436.2021.1886041
5. Kayani, Z. N., Abbas, E., Saddiqe, Z., Riaz, S., Naseem, S., “Photocatalytic, antibacterial, optical and magnetic properties of Fe-doped ZnO nano-particles prepared by sol-gel”, ***Materials***

Science in Semiconductor Processing, Vol. 88, (2018), 109-119. https://doi.org/10.1016/j.mssp.2018.08.003

6. Karthik, K. V., Raghu, A. V., Reddy, K. R., Ravishankar, R., Sangeeta, M., Shetti, N. P., Reddy, C. V., "Green synthesis of Cu-doped ZnO nanoparticles and its application for the photocatalytic degradation of hazardous organic pollutants", ***Chemosphere***, Vol. 287, (2022), 132081. https://doi.org/10.1016/j.chemosphere.2021.132081
7. Zhang, Q., Zhao, X., Libing, D., Shen, H., Liu, R., "Controlling oxygen vacancies and enhanced visible light photocatalysis of CeO_2/ZnO nanocomposites", ***Journal of Photochemistry and Photobiology A: Chemistry***, Vol. 392, (2020), 112156. https://doi.org/10.1016/j.jphotochem.2019.112156
8. Ahmed, A. A. A., Abdulwahab, A. M., Talib, Z. A., Salah, D., Flaifel, M. H., "Magnetic and optical properties of synthesized ZnO–$ZnFe_2O_4$ nanocomposites via calcined Zn–Fe layered double hydroxide", ***Optical Materials***, Vol. 108, (2020), 110179. https://doi.org/10.1016/j.optmat.2020.110179
9. Khosravi, M. D., Ghahari, M., Shafiee Afarani, M., Arabi, A. M., "Synthesis of CuO and CuO/ZnO Composite Powders for Antibacterial, Photocatalytic, and Pigment-Related Applications", ***Advanced Ceramics Progress***, Vol. 8, No. 1, (2022), 1-8. https://doi.org/10.30501/acp.2022.329820.1082
10. Wang, L., Li, J., Wang, Y., Zhao, L., Jiang, Q., "Adsorption capability for Congo red on nanocrystalline MFe_2O_4 (M = Mn, Fe, Co, Ni) spinel ferrites", ***Chemical Engineering Journal***, Vol. 181, (2012), 72-79. https://doi.org/10.1016/j.cej.2011.10.088
11. Amirimehr, A., Ghasemi, E., Fazlali, A., "Rheological Study of Nickel Ferrite Ferrofluid", ***Advanced Ceramics Progress***, Vol. 1, No. 2, (2015), 29-33. https://doi.org/10.30501/acp.2015.90745
12. Mmelesi, O. K., Masunga, N., Kuvarega, A., Nkambule, T. T., Mamba, B. B., Kefeni, K. K., "Cobalt ferrite nanoparticles and nanocomposites: Photocatalytic, antimicrobial activity and toxicity in water treatment", ***Materials Science in Semiconductor Processing***, Vol. 123, (2021), 105523. https://doi.org/10.1016/j.mssp.2020.105523
13. Vaish, G., Kripal, R., Kumar, L., "Comprehensive study of magnetic and optoelectronic properties of $MgFe_2O_4$–TiO_2 nanocomposites", ***Materials Chemistry and Physics***, Vol. 271, (2021), 124911. https://doi.org/10.1016/j.matchemphys.2021.124911
14. Cheng, W., Tang, K., Sheng, J., "Highly Water-Soluble Superparamagnetic Ferrite Colloidal Spheres with Tunable Composition and Size", ***Chemistry–A European Journal***, Vol. 16, No. 12, (2010), 3608-3612. https://doi.org/10.1002/chem.201000014
15. Hong, R., Pan, T., Qian, J., Li, H., "Synthesis and surface modification of ZnO nanoparticles", ***Chemical Engineering Journal***, Vol. 119, No. 2-3, (2006), 71-81. https://doi.org/10.1016/j.cej.2006.03.003
16. Fu, L. S., Xu, C. Y., Wang, W. S., Jiang, J. T., Zhen, L., "Superparamagnetic nickel ferrite colloidal spheres for constructing magnetically responsive photonic crystals", ***Materials Letters***, Vol. 81, (2012), 62-64. https://doi.org/10.1016/j.matlet.2012.04.139
17. Patterson, A. L., "The Scherrer Formula for X-Ray Particle Size Determination", ***Physical Review***, Vol. 56, No. 10, (1939), 978-982. https://doi.org/10.1103/PhysRev.56.978
18. Leshuk, T., Krishnakumar, H., Gu, F., "Size-tunable Fe_3O_4 spherical nanoclusters through a one-pot hydrothermal synthesis", ***Journal of Nanoscience and Nanotechnology***, Vol. 15, No. 7, (2015), 5378-5383. https://doi.org/10.1166/jnn.2015.9003
19. Vijayaprasath, G., Murugan, R., Mahalingam, T., Ravi, G., "Comparative study of structural and magnetic properties of transition metal (Co, Ni) doped ZnO nanoparticles", ***Journal of Materials Science: Materials in Electronics***, Vol. 26, No. 9, (2015), 7205-7213. https://doi.org/10.1007/s10854-015-3346-z
20. Ebrahimi, S., Yarmand, B., Naderi, N., "Effect of the Sulfur Concentration on the Optical Band Gap Energy and Urbach Tail of Spray-Deposited ZnS Films", ***Advanced Ceramics Progress***, Vol. 3, No. 4, (2017), 6-12. https://doi.org/10.30501/acp.2017.90759